JACS
JOURNAL OF THE AMERICAN CHEMICAL SOCIETY

COMMUNICATION

pubs.acs.org/JACS

Structural and Electronic Characterization of Non-Heme Fe(II)−Nitrosyls as Biomimetic Models of the Fe_B Center of Bacterial Nitric Oxide Reductase

Timothy C. Berto,[†] Melissa B. Hoffman,[†] Yuki Murata,[†] Kira B. Landenberger,[†] E. Ercan Alp,[‡] Jiyong Zhao,[‡] and Nicolai Lehnert*[,†]

[†]Department of Chemistry, University of Michigan, 930 North University Avenue, Ann Arbor, Michigan 48109-1055, United States

[‡]Argonne National Laboratory, APS/XFD, 431/D003, Argonne, Illinois 60439, United States

Supporting Information

ABSTRACT: The detoxification of nitric oxide (NO) by bacterial NO reductase (NorBC) has gained much attention as this reaction provides a paradigm as to how NO can be detoxified anaerobically in cells. However, a clear mechanistic picture of how the heme/non-heme active site of NorBC activates NO is lacking, mostly as a result of insufficient knowledge about the properties of the non-heme iron(II)−NO adduct. Here we report the first biomimetic model complexes for this species that closely resemble the coordination environment found in the protein, using the ligands BMPA-Pr and TPA. The systematic investigation of these compounds allowed us to gain key insight into the electronic structure and geometric properties of high-spin non-heme iron(II)−NO adducts. In particular, we show how small changes in the ligand environment of iron could be used by NorBC to greatly modulate the properties, and hence, the reactivity of this species.

Nitric oxide (NO) is an important biomolecule that serves as a signaling and immune defense agent in the human body, and as an intermediate in denitrification. Importantly, since NO is acutely toxic to cells,[1] efficient mechanisms for the detoxification of NO must be in place wherever NO is produced in order to avoid cellular damage. One viable pathway is the reduction of NO to less toxic N_2O, as observed in denitrifying bacteria.[2] To elucidate the biological pathways for control of NO levels in cells, much research has been aimed at understanding one key enzyme, bacterial NO reductase (NorBC).[3] This protein contains a dinuclear active site with both a heme and a non-heme (Fe_B) iron center in close proximity. In the first step of catalysis, each ferrous iron center binds one molecule of NO,[2b] but the following steps remain elusive. The basic properties of the ferrous heme−nitrosyl component of the active site are now well understood.[4] To advance our knowledge of the mechanism of NorBC, it is of critical importance to develop a better understanding of the properties of the non-heme Fe_B(II)−NO adduct. A recent crystal structure of NorBC has clarified the coordination environment of the Fe_B site (Scheme 1) and provides a basis for moving forward in this direction.[5] Here we report the first close spectroscopic and structural model complexes for the Fe_B(II)−NO center of NorBC and systematically elucidate the factors that control the electronic structure, and hence, the reactivity of this species.

Scheme 1. Structural Comparison of the Fe_B Site within NorBC (left) and the Model Complex 1-Cl (right)

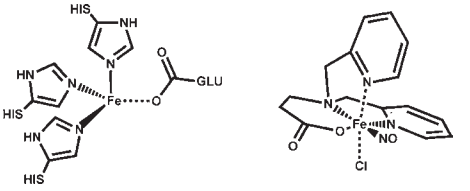

Model complexes aimed at non-heme iron enzymes frequently employ derivatives of the ligand tris(2-pyridylmethyl)amine (TPA).[6] However, this ligand does not accurately model the coordination environment of the Fe_B center of NorBC. We therefore substituted one of the methylpyridyl arms of TPA with a carboxylate group, yielding the biomimetic ligand *N*-propanoate-*N*,*N*-bis(2-pyridylmethyl)amine (BMPA-Pr). As shown in the following, non-heme iron(II)−NO complexes with BMPA-Pr and TPA show amazing versatility of both the complex geometry and the properties of the bound NO unit as a function of small alterations in the counterion and coligand. Synthesis of the BMPA-Pr ligand was carried out via previously published procedures.[7] Metal insertion by reaction with ferrous salts gave yellow-orange complexes [Fe(BMPA-Pr)]X (X = Cl^-, ClO_4^-, I^-, $CF_3SO_3^-$ = OTf^-) with characteristic absorption bands in the 300−450 nm region [Figure S1 in the Supporting Information (SI)]. The isolated iron complexes are EPR-silent in accordance with their Fe(II) oxidation states. Addition of NO gas generates brown complexes [Fe(BMPA-Pr)(NO)]X (**1-X**) that show EPR activity ($S = {}^3/_2$). $[Fe(TPA)(CH_3CN)_2](ClO_4)_2$ was synthesized similarly to published procedures,[8] and exposure to NO gas then yielded $[Fe(TPA)(CH_3CN)(NO)](ClO_4)_2$ (**2**). Interestingly, the ferrous BMPA-Pr precursor complexes show Fe(II)/Fe(III) redox potentials of 200−250 mV vs SHE in CH_3CN, which is very close to the value of 320 mV reported for the Fe_B center of NorBC.[2a] In contrast, the redox potential of the ferrous TPA complex is 860 mV in CH_3CN,[8] indicating that the carboxylate group in BMPA-Pr has a strong influence on the properties of the resulting ferrous complexes. In aqueous media, the Fe(II)/Fe(III) couple for [Fe(BMPA-Pr)]X shifts to potentials of ∼500 mV vs SHE (Table 1). Besides the general

Received: January 11, 2011
Published: June 01, 2011

dx.doi.org/10.1021/ja111693f | *J. Am. Chem. Soc.* 2011, 133, 16714–16717

Table 1. Comparison of Midpoint Potentials[a] for Selected Non-Heme Iron Complexes and Nitrosyl Derivatives

Iron Complex		Fe(II)/Fe(III)
[Fe(BMPA-Pr)]Cl		203/508
[Fe(BMPA-Pr)]ClO_4		200/497
[Fe(BMPA-Pr)]OTf		242/513
[Fe(TPA)$(CH_3CN)_2$]$(ClO_4)_2$[b]		860/−
Nitrosyl Derivative	Fe−NO oxidation[c]	Fe−NO reduction
1-OTf	589/1292	−290/−366
1-ClO_4	609/1323	−296/−386

[a] Values are given in mV vs SHE. The first value was obtained in CH_3CN solvent and the second in H_2O. [b] Data from ref 8. [c] As the oxidations of **1-OTf** and **1-ClO_4** are irreversible, only the oxidation peaks are given.

effect of the solvent dielectric, we believe that this shift is also related to hydrogen-bonding interactions of water with the carboxylate group, which result in a "less anionic" BMPA-Pr ligand and thus a more cationic Fe center [shifting the potential closer to that seen for Fe(TPA) derivatives]. The nitrosyl complexes **1-OTf** and **1-ClO_4** show clear semireversible Fe−NO reductions and an irreversible oxidation peak. Data obtained for **1-Cl** and **2** show multiple redox processes in water and require further study.

Elucidation of the exact coordination environment of the **1-X** complexes (X = Cl^-, OTf^-, ClO_4^-) was carried out by X-ray crystallography. Excitingly, the refined structure of **1-Cl** revealed a geometry very similar to that of the non-heme Fe_B center of NorBC[5] (Figure 1, left), in which the three histidine ligands form a trigonal face and a carboxylate residue occupies a position *trans* to one of the histidine rings. The model **1-Cl** shows a nearly identical coordination environment, with pyridine and amine groups in the place of histidine. The NO and Cl^- ligands then complete an octahedral geometry (Figure 1, left). **1-Cl** shows a bent Fe−N−O unit with an angle of 152° and Fe−NO and N−O distances of 1.783 and 1.154 Å, respectively. The strongly coordinating Cl^- counterion remains bound upon NO addition and prevents coordination of solvent to the Fe center.

In comparison, crystals of both **1-ClO_4** and **1-OTf** show the surprising propensity of these complexes to form unique metallacrown[9] hexamers (Figure 1, right). Here, the open coordination site left by the noncoordinating counterion is not occupied by a solvent molecule. Rather, the carboxylate group of each unit bridges two adjacent iron centers, giving ring structures wherein all six NO moieties point toward the center of the ring. The oxygen atoms of the six NO ligands form an empty octahedron (volume ≈ 20 $Å^3$). The geometries of the individual {Fe(BMPA-Pr)(NO)} units also differ from that seen in **1-Cl**. Whereas **1-Cl** shows a trigonal-facial arrangement of the N-donor groups of BMPA-Pr, **1-OTf** and **1-ClO_4** show the alternative meridional binding mode (see Figure 1). Density functional theory (DFT) calculations show that the total energies of the facial and meridional isomers of **1-Cl** differ by only ∼3 kcal/mol, indicating that the BMPA-Pr ligand can easily reorient its binding mode. The hexameric metallacrowns **1-ClO_4/1-OTf** show average Fe−NO and N−O bond distances of 1.72/1.76 Å and 1.18/1.17 Å, respectively, and an average Fe−N−O angle of 152°/149°. Interestingly, the bridging carboxylate groups in the hexameric structures show equivalent Fe−O distances of ∼2.07 Å to both iron centers, which is slightly longer than the Fe−O bond length of 2.02 Å observed for **1-Cl**. This strong Fe−OCO−Fe linkage causes the hexameric

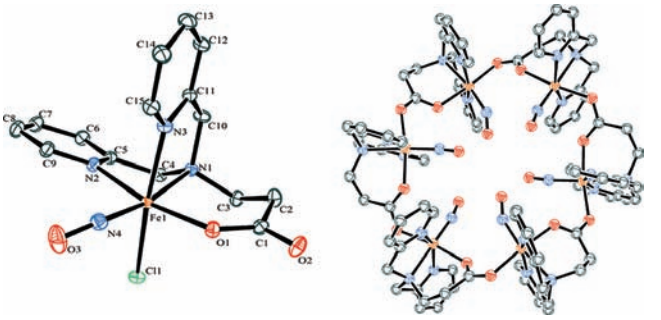

Figure 1. (left) Crystal structure of **1-Cl**, which has a ligand arrangement very close to that seen in the Fe_B center of NorBC. (right) Crystal structure of **1-ClO_4** showing an unexpected metallacrown hexamer. All of the solvent molecules and H atoms have been omitted for clarity. A complete list of geometric parameters is available in the SI.

structures to be quite robust. Our current data indicate that the metallacrown is maintained even in solution.[10]

EPR spectra were recorded for all of the nitrosyls **1-X** and **2**. Both **1-Cl** and **2** show typical $S = {}^3/_2$ signals at liquid He temperatures with effective g values of ∼4 and ∼2 (Figure S3). These data are in accordance with the well-established electronic structure of non-heme ferrous nitrosyls, which show Fe(III)−NO^- ground states where the high-spin (hs) Fe(III) and NO^- ($S = 1$) are antiferromagnetically coupled.[11] Interestingly, the solution EPR spectra of the hexameric complexes **1-OTf** and **1-ClO_4** show evidence of weak electronic coupling between the {Fe(BMPA-Pr)-(NO)} units (Figure S4), further indicating that these hexamers remain intact in solution.

Vibrational spectroscopy was used to further characterize the nature of the Fe−N−O unit in **1-X** and **2**. Importantly, the IR spectra of the **1-X** complexes show N−O stretching frequencies which are significantly affected by small changes in the coordination sphere. **1-Cl** has the lowest energy N−O stretch, ν(N−O), at 1726 cm^{-1} (in the single crystal). Exchange of chloride for iodide shifts ν(N−O) to 1769 cm^{-1}. Noncoordinating counterions such as ClO_4^- and OTf^- further shift ν(N−O) to 1777 and 1784 cm^{-1}, respectively. The N−O stretch of **1-I** is somewhat intermediate, which could result either from iodide being a weaker donor than chloride, or from the formation of a metallacrown structure. Finally, replacing the carboxylate in **1-X** with another pyridine, as in **2**, leads to an N−O stretching frequency of 1810 cm^{-1}. An important hallmark of ferrous non-heme nitrosyls is therefore the dramatic tunability of the N−O bond strength, which results in an impressive 84 cm^{-1} difference between the ν(N−O) values in **2** (1810 cm^{-1}) and **1-Cl** (1726 cm^{-1}) as observed here.[12] Consequently, the carboxylate ligand present in the Fe_B site of NorBC seems to play an important role in tuning the reactivity of the Fe_B−NO complex, and does not simply provide a stable coordination sphere for iron as previously proposed.[3b]

Determination of the Fe−NO stretching modes was challenging as these vibrations are IR-silent and the complexes show decomposition upon laser irradiation. Therefore, to probe the iron-centered vibrations, Nuclear Resonance Vibrational Spectroscopy (NRVS) was employed.[13] NRVS is ideally suited for this purpose, as the spectral intensity of a vibration is proportional to its amount of ^{57}Fe motion with this technique. Through $^{15}N^{18}O$ isotope labeling, the ^{57}Fe−NO stretching vibrations in **1-Cl**, **1-OTf**, and **2** were identified at 484, 495, and 502 cm^{-1}, respectively. While

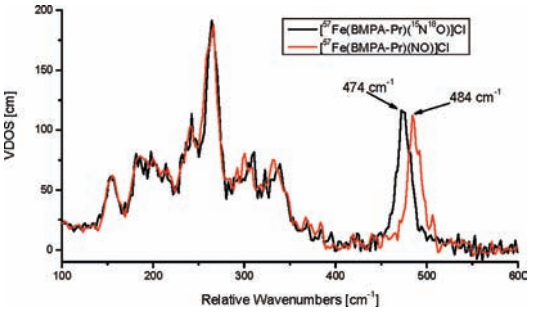

Figure 2. Overlay of the NRVS spectra of ^{57}**1-Cl** containing natural-abundance isotopes NO and $^{15}N^{18}O$. The large isotope-sensitive band at 484 cm^{-1} is assigned to ν(Fe−NO).

analysis of the NRVS data for both ^{57}**1-Cl** (Figure 2) and ^{57}**1-OTf** is straightforward, ^{57}**2** shows a split ^{57}Fe−NO stretch at 495 and 509 cm^{-1}. In view of this, we tentatively assign the "pure" vibration to the average position of ∼502 cm^{-1}. Figure 3 shows a correlation plot of ν(Fe−NO) versus ν(N−O) for all these complexes. Importantly, the observed correlation between ν(Fe−NO) and ν(N−O) is *not* inverse, as would be expected for a change in Fe−NO back-bonding along this series. In fact, a clear direct correlation is observed.

To gain a better understanding of the nature of the Fe−NO bond and the observed trends in Fe−NO and N−O bond strengths (frequencies), DFT calculations were employed. The BP86/TZVP-optimized structure of **1-Cl** shows excellent agreement with experiment; for example, an Fe−NO distance of 1.74 Å and Fe−N−O angle of 153° are observed. The calculated N−O stretching frequency of 1733 cm^{-1} is close to the experimental value of 1726 cm^{-1}. The Fe−NO stretch is overestimated at 522 cm^{-1} relative to experiment (484 cm^{-1}), which is not unusual, as gradient-corrected functionals commonly overestimate metal−ligand covalencies and hence, bond strengths.[14] For the hexameric complexes **1-OTf** and **1-ClO$_4$**, a single {Fe(BMPA-Pr)(NO)} unit was constructed by terminating the carboxylate bridges with Li$^+$ ions. This model also reproduces the experimental geometries well (see Figure S2) and produces ν(Fe−NO) and ν(N−O) values of 530 and 1788 cm^{-1}, respectively. Finally, calculation of the vibrational properties of $[Fe(TPA)(CH_3CN)(NO)]^{2+}$ predicts ν(Fe−NO) and ν(N−O) values of 537 and 1791 cm^{-1}, respectively. Thus, the DFT (BP86/TZVP) results replicate the experimental vibrational frequencies of **1-X** and **2** well and, in particular, reproduce the direct correlation between ν(Fe−NO) and ν(N−O) (Figure 3).

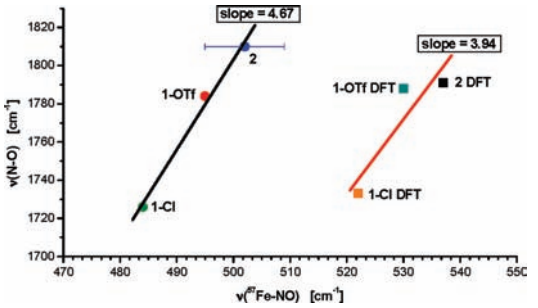

Figure 3. Correlation plot of ν(Fe−NO) vs ν(N−O) for **1-X** and **2**. The experimental (black) and DFT-predicted (red) trends are shown.

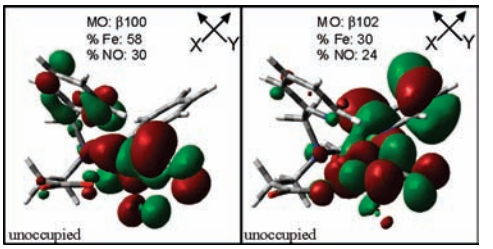

Figure 4. Contour plots of antibonding β-spin MOs showing the interactions of the occupied NO β-π^* orbitals with the d_{xz} and d_{yz} orbitals of iron.

Because of the close agreement between experiment and DFT, the computational results can be used to gain insight into the electronic-structural reasons for the observed vibrational correlation. Analysis of the molecular orbital (MO) diagram of **1-Cl** reveals an electronic-structural description that is in agreement with the hs Fe(III)−NO$^-$ bonding scheme previously proposed.[11] Correspondingly, in the α-spin MO diagram, all of the iron d orbitals are (singly) occupied. In the applied coordinate system (Fe−NO vector corresponding to the z axis), the d_{xz} and d_{yz} orbitals form back-bonds with the two unoccupied α-π^* orbitals of NO, π_v^* and π_h^*. This interaction is relatively weak, as is evident from the corresponding antibonding MOs α102 (72% π_v^*), α103 (33% π_h^*), and α104 (48% π_h^*), which have relatively small iron d-orbital contributions (Figure S5). Notably, the bending of the Fe−N−O unit also allows for back-bonding of π_h^* with d_{z^2}, as can be seen from the occupied MO α100 (41% d_{z^2}, 19% π_h^*). In the β-spin MO diagram, all of the iron d orbitals are empty, whereas the β−π^* orbitals of NO are now occupied, in accordance with the NO$^-$ ($S = 1$) description of the NO ligand. The occupied β−π^* orbitals of NO are ideally suited to donate into the empty β-spin d_{xz} and d_{yz} orbitals of iron. The strength of this interaction is again best estimated from the corresponding antibonding combinations β100 (58% d_{yz/z^2}, 30% π_h^*) and β102 (30% d_{xz}, 24% π_v^*), which show significant iron d-orbital and NO π^* character (see Figure 4). As a result, the π donation from NO$^-$ into the iron β-d_{xz} and β-d_{yz} orbitals is significant. In summary, *NO$^-$ acts as a weak π-acceptor (α-spin) and strong π-donor (β-spin) ligand in these complexes.* The calculated spin density distribution is in agreement with this description, delivering values of +3.19 and −0.64 for Fe and NO, respectively. These values reflect the strong donation of negative (β) spin density from NO to iron and the relatively weak back-donation of positive (α) spin density from iron to NO. Importantly, the direct correlation between the Fe−NO and N−O bond strengths and vibrational frequencies can therefore be explained by variations in the amount of π donation from the NO$^-$ ligand to the iron center. Since this donation originates from N−O antibonding (π^*) orbitals, a strengthening of this interaction (i.e., an increase in donation) results in the strengthening of both the Fe−NO and N−O bonds simultaneously and hence, an increase in both ν(Fe−NO) and ν(N−O). Interestingly, *the observed trend in Figure 3 correlates with the number of anionic ligands bound to the iron center*; which is two for **1-Cl**, one (on average) for **1-OTf**,[15] and none for **2**. Hence, this effect seems to be correlated with the effective nuclear charge of iron, where a more negative iron center is less likely to accept electron donation from bound NO$^-$. Consequently, TPA complexes should exhibit the highest N−O stretching frequencies due of the lack of an anionic donor. The data support this trend, as **2** shows ν(N−O) at 1810 cm^{-1} and the related complex $[Fe(TPA)(BF)(NO)]ClO_4$ containing the

dx.doi.org/10.1021/ja111693f |J. Am. Chem. Soc. 2011, 133, 16714–16717

delocalized, weak anionic benzoylformate (BF) ligand shows ν(N−O) at 1794 cm^{-1}.[16]

To conclude, we have presented structural, spectroscopic, and theoretical data on the first biomimetic model complexes for the non-heme Fe_B(II)−NO adduct of NorBC. Our results have uncovered a surprising tunability of the properties of the Fe−NO bond in these systems based on the number of anionic donors bound to the iron center.[12] This tunability is synthetically easy to access, as simple changes in the coligand and counterion lead to dramatic effects on the Fe−NO unit, as evidenced by the shift of 84 cm^{-1} in ν(N−O) between **1-Cl** and **2**. Notably, the observed shift does not relate to the difference in BMPA-Pr binding mode (see Figure S2). Further vibrational studies show that this tunability in the Fe−NO bond manifests itself as a direct correlation between the Fe−NO and N−O bond strengths (frequencies). Specifically, changes in π donation from the bound NO^- (S = 1) ligand to hs Fe(III) are responsible for the observed correlation. These results have important consequences for NorBC catalysis, as our data suggest that the protein has the ability to control the properties of the Fe_B(II)−NO center in a similar fashion, that is, by adjusting the number and donor strengths (via hydrogen bonding) of anionic ligands bound to the Fe_B center. Unfortunately, ν(N−O) for the Fe_B−NO complex is not known, so comparison with our model systems cannot be made. Considering redox potentials, the Fe_B center is only slightly more oxidizing than our BMPA-Pr model systems in CH_3CN, which indicates (a) that glutamate remains bound to the Fe_B center upon reduction to the ferrous form and (b) that hydrogen bonds to the bound glutamate are likely to be present and responsible for the increase in redox potential. Considering this scenario, we predict that the Fe_B−NO complex of NorBC has properties similar to those of the Fe−NO units in **1-OTf** and **1-ClO_4**. This aspect requires further study.

Initial reactivity studies with five-coordinate [Fe(Porph)(NO)] ($Porph^{2-}$ = TPP^{2-}, T*o*-F_2PP^{2-}) and six-coordinate [Fe(T*o*-F_2PP-BzIM)(NO)] complexes[3e] show no reactivity upon simple mixing of the heme- and non-heme iron−nitrosyls in organic solvents. In view of the fact that these complexes by themselves are also unreactive toward additional NO gas, the frequently cited radical-type N−N coupling mechanism of NorBC is unlikely (compare with ref 14). Current studies are focused on adjusting the redox potentials in the heme- and non-heme iron−nitrosyl complexes to investigate the possibility of (proton-assisted) reductive coupling between the two NO ligands of the heme and non-heme iron components.

■ ASSOCIATED CONTENT

Supporting Information. Synthetic procedures; UV−vis IR, EPR, and NRVS spectra; tables of geometric parameters; MO plots; and crystallographic data (CIF). This material is available free of charge via the Internet at http://pubs.acs.org.

■ AUTHOR INFORMATION

Corresponding Author
lehnertn@umich.edu

■ ACKNOWLEDGMENT

This work was supported by the National Science Foundation (CHE 0846235). We acknowledge Dr. Jeff Kampf (University of Michigan) for his X-ray crystallographic analyses of **1-Cl**, **1-ClO_4**, and **1-OTf**, and funding from NSF grant CHE-0840456 for X-ray instrumentation.

■ REFERENCES

(1) Burney, S.; Tamir, S.; Gal, A.; Tannenbaum, S. R. *Nitric Oxide* **1997**, *1*, 130.

(2) (a) Zumft, W. G. *J. Inorg. Biochem.* **2005**, *99*, 194. (b) Kumita, H.; Matsuura, K.; Hino, T.; Takahashi, S.; Hori, H.; Fukumori, Y.; Morishima, I.; Shiro, Y. *J. Biol. Chem.* **2004**, *279*, 55247.

(3) (a) Xu, N.; Campbell, A. L. O.; Powell, D. R.; Khandogin, J.; Richter-Addo, G. B. *J. Am. Chem. Soc.* **2009**, *131*, 2460. (b) Yeung, N.; Lin, Y. W.; Gao, Y. G.; Zhao, X.; Russell, B. S.; Lei, L.; Miner, K. D.; Robinson, H.; Lu, Y. *Nature* **2009**, *462*, 1079. (c) Collman, J. P.; Yang, Y.; Dey, A.; Decréau, R. A.; Ghosh, S.; Ohta, T.; Solomon, E. I. *Proc. Natl. Acad. Sci. U.S. A.* **2008**, *105*, 15660. (d) Schopfer, M. P.; Wang, J.; Karlin, K. D. *Inorg. Chem.* **2010**, *49*, 6267. (e) Berto, T. C.; Praneeth, V. K. K.; Goodrich, L. E.; Lehnert, N. *J. Am. Chem. Soc.* **2009**, *131*, 17116.

(4) (a) Patchkovskii, S.; Ziegler, T. *Inorg. Chem.* **2000**, *39*, 5354. (b) Cheng, L.; Richter-Addo, G. B. In *The Porphyrin Handbook*; Kadish, K. M., Smith, K. M., Guilard, R., Eds.; Academic Press: New York, 2000; Vol. 4, Chapter 33, pp 219−291. (c) Wyllie, G. R. A.; Scheidt, R. *Chem. Rev.* **2002**, *102*, 1067. (d) Coyle, C. M.; Vogel, K. M.; Rush, T. S.; Kozlowski, P. M.; Williams, R.; Spiro, T. G.; Dou, Y.; Ikeda-SaitoM.; Olson, J. S.; Zgierski, M. Z. *Biochemistry* **2003**, *42*, 4896. (e) Zhang, Y.; Gossman, W.; Oldfield, E. *J. Am. Chem. Soc.* **2003**, *125*, 16387. (f) Wyllie, G. R. A.; Schulz, C. E.; Scheidt, W. R. *Inorg. Chem.* **2003**, *42*, 5722. (g) Ford, P. C.; Laverman, L. E. *Coord. Chem. Rev.* **2005**, *249*, 391. (h) Wasser, I. M.; Huang, H.; Moënne-Loccoz, P.; Karlin, K. D. *J. Am. Chem. Soc.* **2005**, *127*, 3310. (i) Praneeth, V. K. K.; Näther, C.; Peters, G.; Lehnert, N. *Inorg. Chem.* **2006**, *45*, 2795. (j) Silvernail, N. J.; Barabanschikov, A.; Sage, J. T.; Noll, B. C.; Scheidt, W. R. *J. Am. Chem. Soc.* **2009**, *131*, 2131. (k) Silvernail, N. J.; Olmstead, M. M.; Noll, B. C.; Scheidt, W. R. *Inorg. Chem.* **2009**, *48*, 971. (l) Lehnert, N.; Galinato, M. G. I.; Paulat, F.; Richter-Addo, G. B.; Sturhahn, W.; Xu, N.; Zhao, J. *Inorg. Chem.* **2010**, *49*, 4133. (m) Lehnert, N.; Sage, J. T.; Silvernail, N. J.; Scheidt, W. R.; Alp, E. E.; Sturhahn, W.; Zhao, J. *Inorg. Chem.* **2010**, *49*, 7197.(n) Lehnert, N.; Berto, T. C.; Galinato, M. G. I.; Goodrich, L. E., In *The Handbook of Porphyrin Science*; Kadish, K. M., Smith, K. M., Guilard, R., Eds.; World Scientific: Singapore, 2011; Vol. 14, Chapter 63, pp 1−247.

(5) Hino, T.; Matsumoto, Y.; Nagano, S.; Sugimoto, H.; Fukumori, Y.; Murata, T.; Iwata, S.; Shiro, Y. *Science* **2010**, *330*, 1666.

(6) (a) Que, L., Jr. *Acc. Chem. Res.* **2005**, *40*, 493. (b) Friedle, S.; Reisner, E.; Lippard, S. J. *Chem. Soc. Rev.* **2010**, *39*, 2768.

(7) Carvalho, N. M. F.; Horn, A., Jr.; Bortoluzzi, A. J.; Drago, V.; Antunes, O. A. C. *Inorg. Chim. Acta* **2006**, *359*, 90.

(8) Zang, Y.; Kim, J.; Dong, Y.; Wilkinson, E. C.; Appelman, E. H.; Que, L., Jr. *J. Am. Chem. Soc.* **1997**, *119*, 4197.

(9) Lah, S. M.; Pecoraro, V. L. *J. Am. Chem. Soc.* **1989**, *111*, 7258.

(10) This claim is made on the basis of preliminary solution IR spectra in which the position of ν(N−O) does not shift relative to that of the crystalline sample.

(11) Brown, C. A.; Pavlosky, M. A.; Westre, T. E.; Zhang, Y.; Hedman, B.; Hodgson, K. O.; Solomon, E. I. *J. Am. Chem. Soc.* **1995**, *117*, 715.

(12) As the noncoordinating counterions are not bound directly to the Fe center, their presence indirectly affects the coordination sphere of Fe by limiting the number of anionic ligands bound to the Fe center.

(13) Scheidt, W. R.; Durbin, S. M.; Sage, J. T. *J. Inorg. Biochem.* **2005**, *99*, 60.

(14) Goodrich, L. E.; Paulat, F.; Praneeth, V. K. K.; Lehnert, N. *Inorg. Chem.* **2010**, *49*, 6293.

(15) As the carboxylate groups are equally bridged between two Fe centers in **1-OTf**, the net anionic effect is comparable to having approximately one unshared carboxylate ligand bound to the Fe center.

(16) Chiou, Y.-M.; Que, L., Jr. *Inorg. Chem.* **1995**, *34*, 3270.